magnetochemistry

MDPI

Article

Controlling the Magnetic Properties of $La_{0.9}A_{0.1}Mn_{0.9}Cr_{0.1}O_3$ (A: Li, K, Na) Powders and Ceramics by Alkali Ions Doping

Paweł Głuchowski [1,2,*], Ruslan Nikonkov [1], Daniela Kujawa [1], Wiesław Stręk [2], Tomas Murauskas [3], Andrius Pakalniškis [3], Aivaras Kareiva [3], Andrii Yaremkevych [4], Olena Fesenko [4], Aliaksandr Zhaludkevich [5] and Dmitry Karpinsky [5]

1 Nanoceramics Inc., Okolna 2, PL-50422 Wroclaw, Poland; r.nikonkov@nanoceramics.pl (R.N.); d.kujawa@nanoceramics.pl (D.K.)
2 Institute of Low Temperature and Structural Research PAS, Okolna 2, PL-50422 Wroclaw, Poland; w.strek@intibs.pl
3 Institute of Chemistry, Vilnius University, Universiteto g. 3, LT-01513 Vilnius, Lithuania; tomas.murauskas@chf.vu.lt (T.M.); andrius.pakalniskis@chgf.vu.lt (A.P.); aivaras.kareiva@chgf.vu.lt (A.K.)
4 Institute of Physics NAS of Ukraine, Nauky Ave, 46, UA-02000 Kyiv, Ukraine; andeyjaremkevich@gmail.com (A.Y.); fesenko.olena@gmail.com (O.F.)
5 Namangan Engineering-Construction Institute, Islam Karimov Street 12, Namangan UZ-160103, Uzbekistan; zheludkevich27@gmail.com (A.Z.); dmitry.karpinsky@gmail.com (D.K.)
* Correspondence: p.gluchowski@nanoceramics.pl

Abstract: Nanocrystalline $La_{0.9}A_{0.1}Mn_{0.9}Cr_{0.1}O_3$ (A: Li, K, Na) powders have been synthesized by combustion method. The powders were used to prepare ceramics by high-pressure low-temperature sintering technique. For all samples the structure, elemental composition and morphology were studied using X-ray diffraction (XRD), Raman spectroscopy, Energy-Dispersive X-ray Spectroscopy (EDS) and Scanning electron microscopy (SEM). Magnetic properties were studied using magnetometry methods and the valency changes of the cations after alkali ions doping were studied using X-ray photoelectron spectroscopy (XPS). The influence of the sintering pressure on the structural and magnetic properties of the manganites doped with different alkali ions and chromium was also investigated. Magnetization properties were studied as a function of sintering pressure and type of the dopant. Chemical doping with alkali ions as well as external pressure significantly changed the magnetic properties of the compounds. It was found that the magnetic properties of the manganites could be predictably modified through the use of a suitable dopant element.

Keywords: multiferroic; manganites; nanopowders; ceramics; alkaline ions; doping; magnetization; XPS

Citation: Głuchowski, P.; Nikonkov, R.; Kujawa, D.; Stręk, W.; Murauskas, T.; Pakalniškis, A.; Kareiva, A.; Yaremkevych, A.; Fesenko, O.; Zhaludkevich, A.; et al. Controlling the Magnetic Properties of $La_{0.9}A_{0.1}Mn_{0.9}Cr_{0.1}O_3$ (A: Li, K, Na) Powders and Ceramics by Alkali Ions Doping. *Magnetochemistry* **2023**, *9*, 140. https://doi.org/10.3390/magnetochemistry9060140

Academic Editor: Kamil Gareev

Received: 17 April 2023
Revised: 19 May 2023
Accepted: 22 May 2023
Published: 25 May 2023

1. Introduction

The term multiferroic was first used in 1993 in Ascona, where Hans Schmid [1] used it to refer to materials that combine at least two of the primary ferroic states in one phase, i.e., ferroelectricity, ferroelasticity and ferromagnetisms [1,2]. Presently, four classes of multiferroics can be distinguished and are divided based on the different ways ferroelectricity is facilitated in them. The ferroelectricity may be caused by magnetic field, geometry, charge ordering or lone pair electrons [3–5]. The ideal example that shows a clear relation between structure and magnetic order is a magnetic insulator such as $LaMnO_3$ [6]. This structure belongs to manganite groups, which are a mix of manganese oxides which crystalize in a perovskite structure. The manganites have the formula $ABO_{(3\pm\delta)}$; where A is a lanthanide element and B is manganese, the stoichiometry is related to the oxygen excess or deficiency [7]. The main advantage of the perovskite structure is the possibility of exchanging part of the cations without breaking its crystal structure. It is known that $LaMnO_3$ has an orthorhombic structure, which allows for tilting modes and Jahn–Teller

distortion [8]. Exchange of trivalent ions in A position can modify Mn ion valency (from trivalent to tetravalent) which may change this paramagnetic insulator to ferromagnetic conductor or lead to a coexistence of mixed magnetic phases [9]. The proposed mechanism of conductivity in manganites was based on the double exchange between Mn^{3+} and Mn^{4+} via oxygen with strong electron phonon coupling [10]. The hole doped $LaMnO_3$ can show the transition from paramagnetic to antiferromagnetic, from paramagnetic to ferromagnetic and also from ferromagnetic to antiferromagnetic phase and is strongly dependent on hole concentration [11–14]. Such doping can be achieved when the trivalent La^{3+} ions are changed with divalent alkali earth ions, which can transform Mn^{3+} ions to Mn^{4+} ions. The transition to ferromagnetism may also be stimulated by exchange of La^{3+} ions with monovalent alkali ions. This in principle should introduce more holes to the structure in comparison to divalent ions [15]. It was found that manganates doped with mono- and many divalent alkali ions are very sensitive to applied external pressure. The hydrostatic pressure changes Curie temperature, cell parameters, increases band gap energy and weakens electron–phonon coupling [16,17]. Another way to alter the manganite properties is by doping with transition metal ions that would change the bandwidth and bond angle between manganese ions [18] and in consequence change the conductivity mechanism. Troyanchuk and Sun showed that partial substitution of manganese by chromium ions leads to a decrease in metallic-insulating (M-I) transition temperature [19,20], and Raveau et al. [21] demonstrated that chromium and cobalt doping leads to stimulated insulator–metal transition in the antiferromagnetic phase in $Pr_{0.5}Ca_{0.5}Mn_{1-x}Cr_xO_3$ without the use of the magnetic field. In $LnMn_{1-x}Cr_xO_3$ perovskite, the substitution of manganese by chromium leads to a transition from antiferromagnetic to ferromagnetic phase with no metallic properties [18–20,22,23]. The ferromagnetic state is possibly caused by the double exchange between manganese and chromium ions, which have almost the same electron configuration as Mn^{4+} ions [24,25]. In manganites doped with chromium, a decrease in Curie temperature, increase resistivity and decrease temperature of transition from metal to semiconductor can be observed with increase in chromium concentration [26–31].

In this work, we continue our systematic work, where the manganites were doped with alkali ions [32] and then doped with cobalt ions [33]. The results obtained in our previous works have shown that chemical doping with alkali metal ions and Co ions, along with the different synthesis methods, can be considered an effective tool for the controllable modification of the electronic configuration of the Mn and Co ions, and thus, the functional properties of the doped manganites. The aim of the actual work is to check the mentioned means for controllable modification of the magnetic properties of the manganites doped with an alkali metal and Cr ions.

2. Materials and Methods

The $La_{0.9}A_{0.1}Mn_{0.9}Cr_{0.1}O_3$ (A: Li, K, Na) were synthesized using the combustion method [34]. The combustion method was chosen for sample preparation because, unlike sol-gel or precipitation methods, it allows for a quick (about 2 h of the whole process) and low-cost synthesis of a structurally pure material. In addition, it is an easily scalable method that allows you to obtain powder in semi-industrial quantities. As a source of precursors, a series of nitrates were used ($La(NO_3)_3 \bullet 6H_2O$, $Mn(NO_3)_2 \bullet 4H_2O$, $Cr(NO_3)_2 \bullet 9H_2O$, $LiNO_3$, $NaNO_3$ or KNO_3). The molar ratio of lanthanum to alkali ions and manganese to chromium was 0.9 to 0.1. The nitrates were mixed with an excess of 10% molten stearic acid and kept at 140 °C under continuous stirring. Stearic acid has a low melting point, prevents the hydrolysis of the prepared structure and acts as a complexing agent; therefore, it helps lower the combustion synthesis temperature. After 2 h, the obtained gel was placed in a furnace heated up to 500 °C. After a short while, the gel ignited spontaneously with the release of a large number of gases and resulting in a black foam-like structure. The foam was ground and calcined at 700 °C for 1 h. After calcination, all powders were ground and taken for further experiments and ceramic sintering. The ceramics were prepared using

a high-pressure, low-temperature sintering technique [35]. The ceramics were sintered at 8 GPa and 500 °C for 1 min.

The structure of the powders and ceramics were measured and analyzed by powder X-ray diffraction (XRD) using a PANalytical X'Pert diffractometer (Malvern Panalytical, Almelo, The Netherlands) with Ni-filtered CuK_λ radiation, λ = 0.15418 nm. Raman investigations were performed in back-scattering geometry using a Renishaw InVia Raman microscope equipped with a confocal DM 2500 Leica optical microscope and CCD detector (Renishaw plc, Wotton-under-Edge, United Kingdom). A 632 nm line from the HeNe laser was used as an excitation source. The spectra were recorded in five scans with a 90 s exposure time, 1 mW of applied power and 50× magnification. EDS analysis was performed using a Hitachi TM3000 microscope (Hitachi, Tokyo, Japan) under 8.5 mm working distance and 15 kV accelerating voltage. The data were collected during a period of 1 h for each sample. An XPS measurement was performed, allowing us to measure the composition of a deeper and larger area of the sample, as the surface analysis results could contain errors or uncertainties due to the inhomogeneity of the sample and the EDS measurement being taken from a single point. The XPS analyses were carried out with a Kratos Axis Supra spectrometer, using a monochromatic Al K(alpha) source (25 mA, 15 kV). XPS can detect all elements except hydrogen and helium, it probes the surface of the sample to a depth of 5–7 nm, and it has detection limits ranging from 0.1 to 0.5 atomic percent depending on the element. The instrument work function was calibrated to give a binding energy (BE) of 83.96 eV for the Au 4f7/2 line for metallic gold, and the spectrometer dispersion was adjusted to give a BE of 932.62 eV for the Cu 2p3/2 line of metallic copper. The Kratos charge neutralizer system was used on all specimens to minimize the impact of sample charging (buildup of surface potential) during data acquisition to enable photoelectron lines to appear nearly at the expected binding energy without sample damage or peak distortion. Survey scan analyses were carried out with an analysis area of 300 × 700 microns and a pass energy of 160 eV. High resolution analyses were carried out with an analysis area of 300 × 700 microns and a pass energy of 20 eV. Spectra have been charge-corrected to the main line of the carbon 1s spectrum (adventitious carbon) set to 284.8 eV. Spectra were analyzed using CasaXPS software (version 2.3.23rev1.1R, Casa Software Ltd., Teignmouth, UK). The magnetic properties of the powders and ceramics were checked, using highly sensitive and precise Physical Properties Measurement Systems from Cryogenic Ltd. (London, UK) in magnetic fields up to ±14 T at 5 K.

3. Results

3.1. Structure and Morphology

The crystal structure of the $La_{0.9}A_{0.1}Mn_{0.9}Cr_{0.1}O_3$ compounds of both series (powders and ceramics) was analyzed using the results of X-ray diffraction measurements performed at room temperature (Figure 1). The crystal structure and the unit cell parameters have been evaluated by Rietveld refinement using X'pert HighScore Plus software (Malvern Panalytical, Malvern, United Kingdom) [36]. The diffraction data testifies to the formation of single-phase compounds without any presence of impurity phases. The diffraction patterns of all the compounds were refined using rhombohedral symmetry with the space group *R-3c*. The difference in the structure of the compounds under study and the initial compound $LaMnO_3$ having orthorhombic symmetry [37] denotes the dopant-induced changes in the geometry of oxygen octahedra specific for the compounds $LaMnO_{(3\pm\delta)}$ [38]. A slight shift in reflections can also be observed compared to the reference based on pure manganate. This shift is attributed to a symmetry disorder resulting from the substitution of lanthanum and manganese with alkaline and chromium ions, respectively. Chemical doping with Li, Na and K ions leads to an increase in the unit cell parameters (Table 1) proportional to the ionic radius of the dopant ions while also keeping the rhombohedral symmetry. The application of high pressure notably diffuses the reflections on the diffraction patterns of the compounds pointing towards much smaller crystallite size and increasing the strains in the compounds, which notably affects the magnetic properties of the compounds as shown

in the next section. It is known, that variation in the particle size can drastically affect the value of magnetization as well as magnetic transition temperature of the manganite and can be considered as an effective method for the modification of the functional properties of complex oxide systems [39,40]. In the manganites, a decrease in the crystallite size leads to a reduction in the magnetization [41] by a disruption of the long-range ferromagnetic interactions occurring in volume and especially in the surface layer of the crystallites. The decrease in the crystallite size was observed already by us [42,43], and is related to the decomposition of the surface layer of the nanocrystallite and decrease in the size of the core. Additionally, it can be observed that for the ceramics at high diffraction angles, the background strongly increases, this may be potentially related to the reflection mode of measurement made on non-parallel surfaces of the small pieces of the ceramics. However, in all cases, it can be seen that the reflections correspond to the rhombohedral structure of $LaMnO_3$ without any impurities.

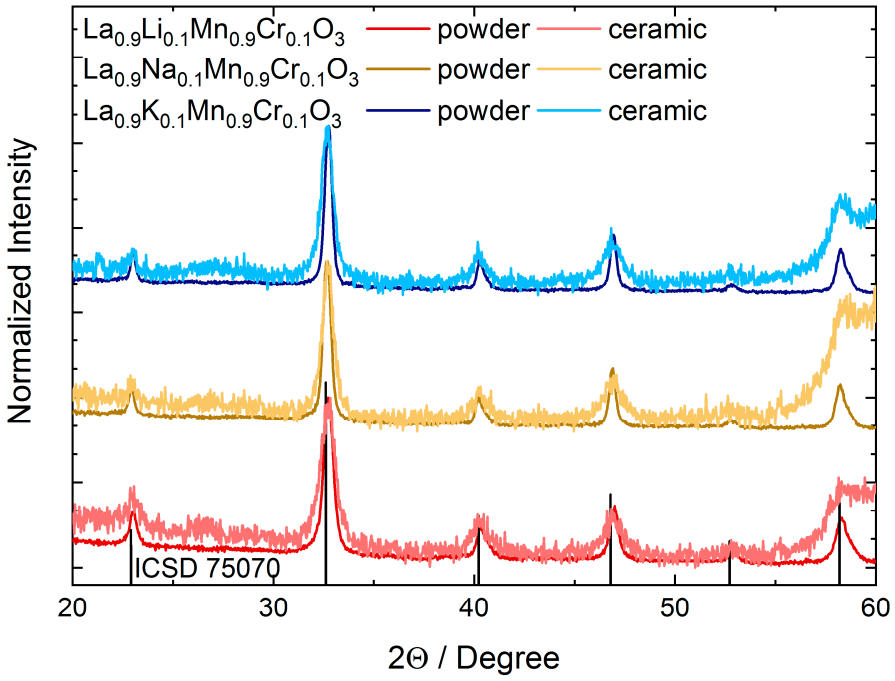

Figure 1. XRD patterns of $La_{0.9}A_{0.1}Mn_{0.9}Cr_{0.1}O_3$ powders and ceramics.

Table 1. Crystal structure parameters and interatomic distances calculated for $La_{0.9}A_{0.1}Mn_{0.9}Cr_{0.1}O_3$ powders and ceramics from XRD data.

	Size	Strains	a, b	c	V	Atomic Distance		
						Mn-O(1)	La-O(1)	La-O(2)
	nm	%	Å	Å	Å^3	Å		
Powders								
$La_{0.9}Li_{0.1}Mn_{0.9}Cr_{0.1}O_3$ R_{exp} = 2.0631, GOF = 2.692	26	0.222	5.496(7)	13.32(3)	348.6(2)	1.957(5)	2.744(1)	2.463(1)
$La_{0.9}Na_{0.1}Mn_{0.9}Cr_{0.1}O_3$ R_{exp} = 2.0317, GOF = 2.4394	34	0.18	5.496(4)	13.34(0)	349.0(1)	1.958(2)	2.746(3)	2.462(9)
$La_{0.9}K_{0.1}Mn_{0.9}Cr_{0.1}O_3$ R_{exp} = 2.0565, GOF = 2.4711	37	0.177	5.503(0)	13.36(4)	350.4(8)	1.961(0)	2.750(6)	2.465(9)
Ceramics								
$La_{0.9}Li_{0.1}Mn_{0.9}Cr_{0.1}O_3$ R_{exp} = 4.6257, GOF = 6.5642	13	0.686	5.505(2)	13.36(3)	350.7(5)	1.961(6)	2.751(9)	2.467(0)
$La_{0.9}Na_{0.1}Mn_{0.9}Cr_{0.1}O_3$ R_{exp} = 5.8594, GOF = 5.2561	16	0.672	5.482(5)	13.44(4)	349.9(6)	1.959(8)	2.758(0)	2.456(7)
$La_{0.9}K_{0.1}Mn_{0.9}Cr_{0.1}O_3$ R_{exp} = 5.3762, GOF = 4.2687	18	0.892	5.488(2)	13.41(3)	349.9(0)	1.942(8)	2.719(8)	2.447(7)

R_{exp}—Expected Rietveld R-factor, GOF—goodness of fit.

Group theory provides 24 Raman active modes ($7A_g + 5B_{1g} + 7B_{2g} + 5B_{3g}$) in a $LaMnO_3$ orthorhombic crystal structure [44]. At the same time, the heating that occurs from laser radiation results in a structural transformation toward the rhombohedral phase in which only five Raman modes ($A_{1g} + 4E_g$) are active [45]. The results obtained for $La_{0.9}A_{0.1}Mn_{0.9}Cr_{0.1}O_3$ (A: Li, Na, K) powders and ceramics are consistent with previous studies of similar perovskite structures, such as $LaMnO_3$ [45]. However, in our study, we observed only three E_g modes (Figure 2) and a shift of the Raman peak position to higher frequencies with the decrease in the atomic nucleus size of the doping alkali metals (Table 2). This can be explained by the substitution of La atoms. As the crystal lattice is compressed, the force constant remains the same and the Raman shift increases. This effect has less impact on E_{g4} (out-of-phase stretching) than E_{g3} (pure oxygen bending vibration) modes, which explains the fact that the Δ between E_{g4} and E_{g3} is also decreased.

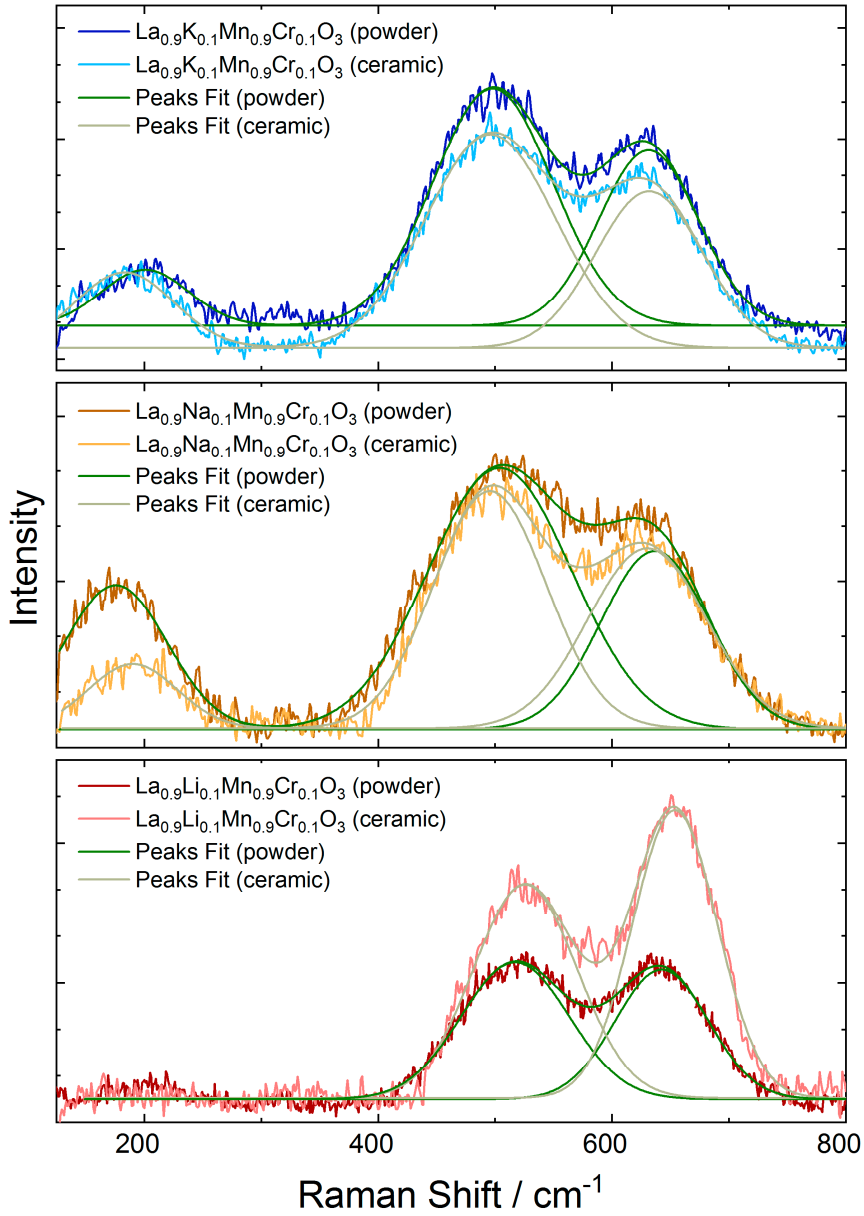

Figure 2. Raman spectra of $La_{0.9}A_{0.1}Mn_{0.9}Cr_{0.1}O_3$ (A: Li, Na, K) powders and ceramics.

For the prepared ceramics and powders doped with different alkali ions as well as chromium, an energy dispersive X-ray spectroscopy analysis (EDS) was performed (Figure 3). The characterization was performed in order to evaluate the elemental distri-

bution and confirm whether their segregation on the grain boundaries had occurred. The elemental distribution maps can be seen in Figure 3. From the given data, we can conclude that no segregation occurred and that the elements were evenly distributed in both ceramic and powder compounds. The ratios of different elements were also measured. No significant differences were observed in the case of the powder-form compounds. A distinctly smaller amount of chromium was measured in the K- and Li-doped ceramics. This could be related to the slight inhomogeneity caused by the application of high pressure. The other dopant concentrations were measured to be around 10%, which is in good accordance with the expected values. However, the amount of lithium was not measured as, in this case, the ion was too light and could not be detected using EDS.

Table 2. Energies (cm^{-1}) and symmetry assignments of Raman-active phonons observed in the Raman spectra of $La_{0.9}A_{0.1}Mn_{0.9}Cr_{0.1}O_3$ (A: Li, Na, K) powders and ceramics.

Raman Modes	E_{g2}	E_{g3}	E_{g4}	Δ
	La	Bending	Antistretching	
		cm^{-1}		
		Powder		
$LaMnO_3$ [44]	198	490	612	122
$La_{0.9}Li_{0.1}Mn_{0.9}Cr_{0.1}O_3$	-	517	643	126
$La_{0.9}Na_{0.1}Mn_{0.9}Cr_{0.1}O_3$	177	504	637	133
$La_{0.9}K_{0.1}Mn_{0.9}Cr_{0.1}O_3$	185	496	632	136
		Ceramic		
$La_{0.9}Li_{0.1}Mn_{0.9}Cr_{0.1}O_3$	-	525	653	128
$La_{0.9}Na_{0.1}Mn_{0.9}Cr_{0.1}O_3$	191	495	630	135
$La_{0.9}K_{0.1}Mn_{0.9}Cr_{0.1}O_3$	201	497	632	135

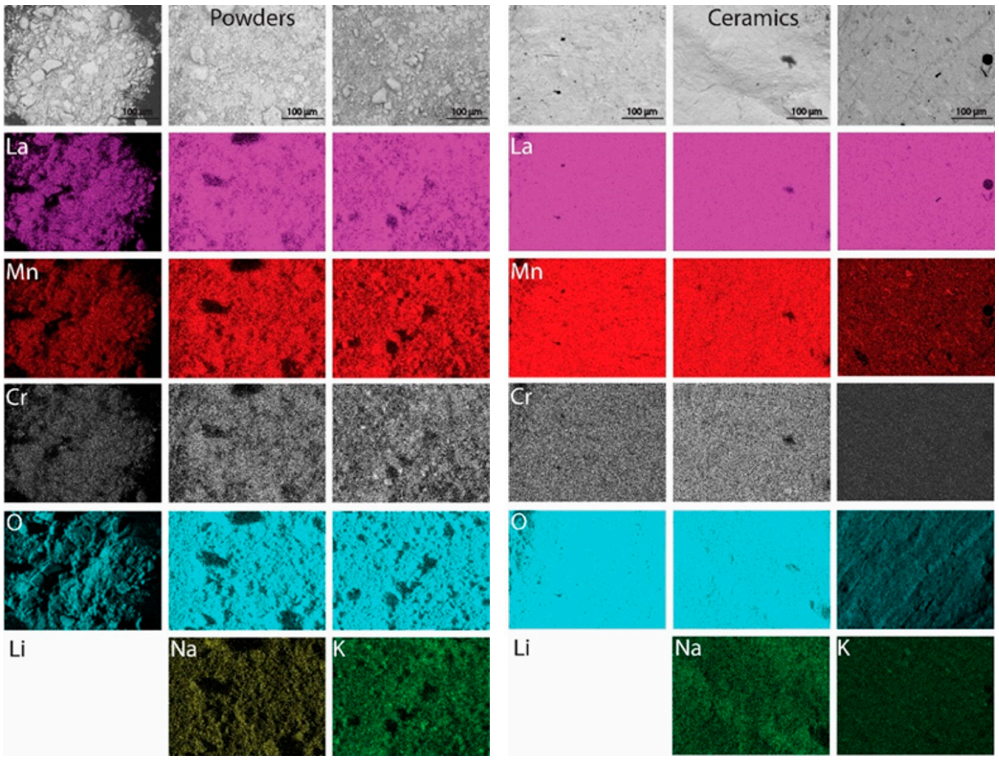

Figure 3. Energy dispersive spectroscopy (EDS) maps of $La_{0.9}A_{0.1}Mn_{0.9}Cr_{0.1}O_3$ powders (**a**) and ceramics (**b**).

3.2. Oxidation States of Mn and Cr Ions

The XPS analysis was carried out for all of the $La_{0.9}A_{0.1}Mn_{0.9}Cr_{0.1}O_3$ powders and ceramics (Figures 4 and 5) and allowed us to clarify the oxidation state of the Mn and Cr ions depending on the chemical composition and the synthesis method. It is known that electronic configuration and, thus, the oxidation state of the Mn ions is a critical issue in determining the type of exchange interactions formed in the manganites [46,47]. The results obtained showed that there was very little quality literature on the exact fitting of Mn2p spectra. Additionally, manganese 2p transitions exhibited multiple splittings due to unpaired electrons, which complicates any kind of analysis. It is possible to analyze Mn^{4+} systems with impurities of Mn^{3+} to some extent, but it is not the case in mixed manganites, which are also doped with two additional elements. It is worth mentioning that Mn^{3+} and Mn^{4+} states show very similar chemical shifts. Therefore, the analysis of Mn2p is at the very least questionable. However, in our case just to get a sense of the possible chemistry of compounds, standard peaks of manganite (MnOOH- as a source of Mn^{3+}) and Pyrolusite (MnO_2- as a source of Mn^{4+}) were used fixing their area ratios and fixing their positions. Approximate amounts of Mn^{3+} and Mn^{4+} were calculated [48] and presented in Table 3. The ratios of Mn^{3+} and Mn^{4+} correlate well with the energy difference between Mn 3s peaks. The peak energy separation between Mn 3s peaks (delta E) observed in the spectra is often reported to correlate with Mn^{4+} and Mn^{3+} ratio as discussed in the literature [49,50]. However, this should also be used very cautiously since other Mn ligands give rise to very different values [48]. In this case, the homogeneous elemental distribution is achieved in all samples through the sol-gel procedure, allowing for atomic-level mixing. This method is commonly used in compounds prepared by sol-gel synthesis. Considering the changes in oxidation states, it is observed that prior to the application of high pressure, the oxidation states remain relatively close regardless of the alkali metal used. It is worth noting that other researchers have also reported similar results, particularly concerning the oxidation state of Mn ions. Similar findings were obtained through Co and Cu doping, where 20% of Co and Cu were introduced instead of Mn, resulting in Mn^{4+}/Mn^{3+} ratios of 0.62 for Cu and 0.55 for Co [51], which are comparable to the compounds in this study. Similarly, in the case of K doping alone, Yolanda Ng Lee et al. found that at 10% doping, the amount of Mn^{4+} was around 32% [52]. However, conflicting results can be found in the literature as well. For instance, in the case of 20% Sr doping in La, the Mn^{4+}/Mn^{3+} ratio was reported to be 1.77 [53], which was significantly higher than what was observed in our work, even considering the larger charge difference in this case. This difference could be attributed to the presence of chromium or the ionic radius disparity between Sr and alkali metals. Furthermore, there are reports of Mn^{2+} being present in the $LaMnO_3$ system doped with K and Ce, although it was not observed in our case [54]. Regarding the effects of high pressure on the oxidation states in $LaMnO_3$, it is challenging to find relevant information in the literature, making comparisons difficult. Ceramic samples seemed to have a trace of Mn^{2+} due to evident satellites indicating this state; however, it was not included due to a weak signal. However, it is worth noting that ceramics seem to possess an overall larger amount of Mn^{3+} ion compared to powders. Similarly, as well, they show a higher amount of Cr^{3+} as compared to Cr^{6+} (except for the Li-doped ceramics). The deviation in the oxidation states may be caused by the modification carried out on the surface of the ceramics when high pressure is applied, and the crystal structure is partially destroyed, thus providing an easier partial reduction in the oxidation states at the surface.

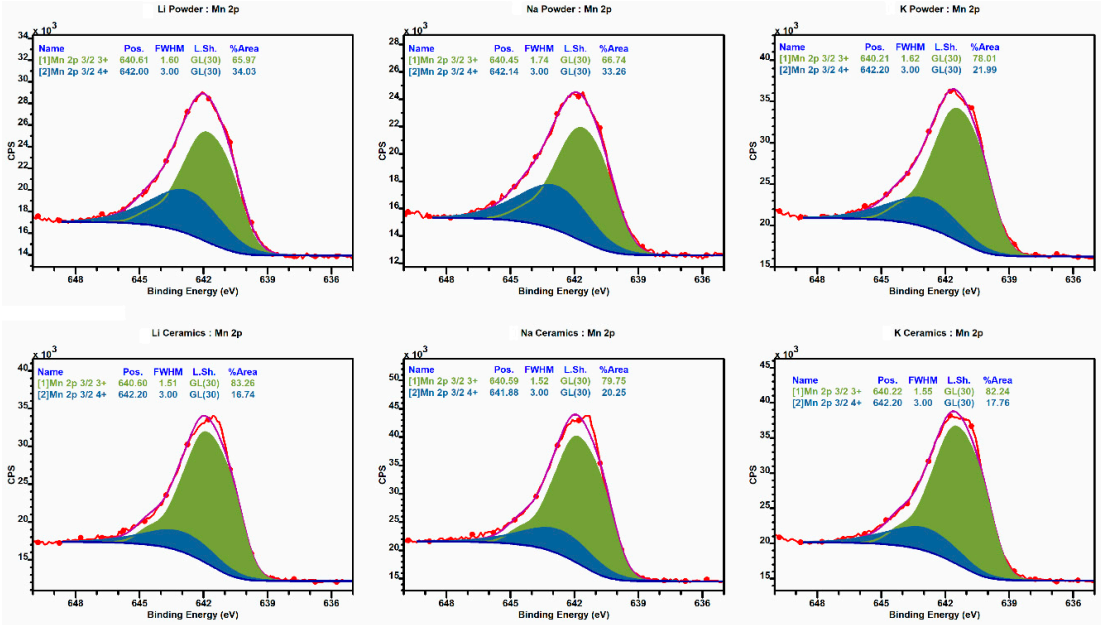

Figure 4. Fitted XPS spectra in the range of 650 eV to 636 eV denoting manganese oxidation sates and their relative amounts.

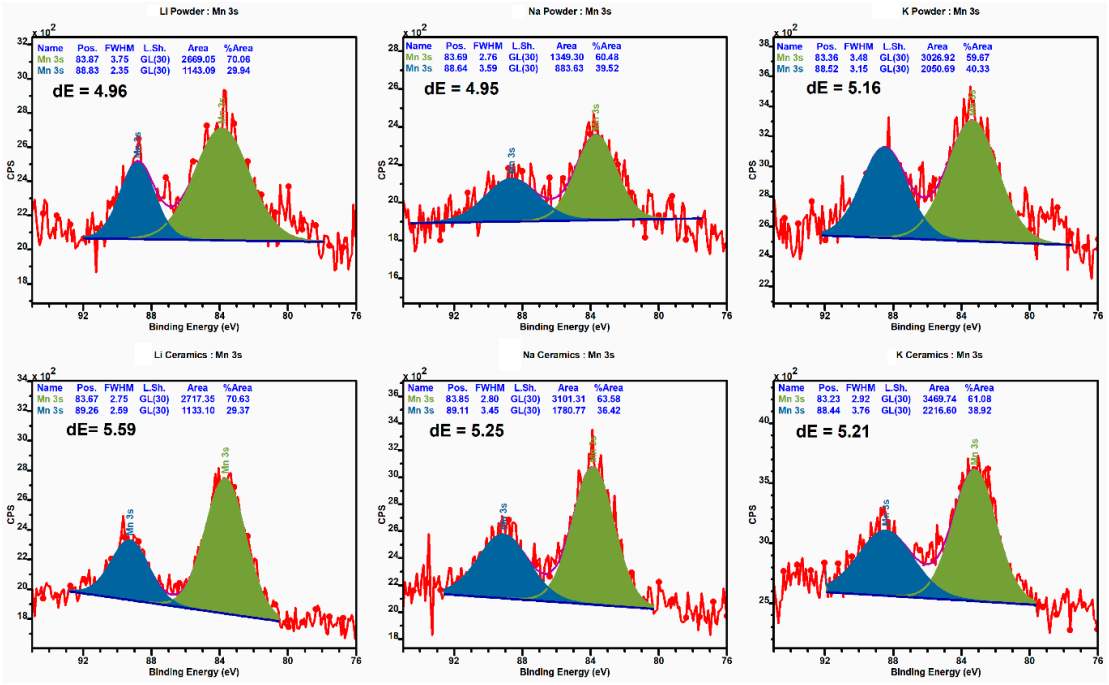

Figure 5. Fitted XPS spectra in the range from 95 eV to 76 eV denoting manganese 3s orbital and calculated dE values.

Table 3. Oxidation state of Mn and Cr ions in $La_{0.9}A_{0.1}Mn_{0.9}Cr_{0.1}O_3$ powders and ceramics.

	Mn Oxidation State (%)		**Cr Oxidation State (%)**	
	3+	**4+**	**3+**	**6+**
		Powder		
$La_{0.9}Li_{0.1}Mn_{0.9}Cr_{0.1}O_3$	66.0	34.0	62.1	37.9
$La_{0.9}Na_{0.1}Mn_{0.9}Cr_{0.1}O_3$	66.7	33.3	53.9	46.1
$La_{0.9}K_{0.1}Mn_{0.9}Cr_{0.1}O_3$	78.0	22.0	50.4	49.6

Table 3. *Cont.*

	Mn Oxidation State (%)		Cr Oxidation State (%)	
	3+	**4+**	**3+**	**6+**
		Ceramic		
$La_{0.9}Li_{0.1}Mn_{0.9}Cr_{0.1}O_3$	83.3	16.7	40.8	59.2
$La_{0.9}Na_{0.1}Mn_{0.9}Cr_{0.1}O_3$	79.8	20.2	85.4	14.6
$La_{0.9}K_{0.1}Mn_{0.9}Cr_{0.1}O_3$	82.2	17.8	78.3	21.7

3.3. Magnetic Properties

Magnetization measurements performed for the compounds have allowed the estimation of an evolution of magnetic structure depending on the dopant element. The mixed magnetic state of the initial compounds is associated with a deficient cation content formed during the synthesis procedure thus leading to the formation of competing positive and negative exchange interactions between isovalent and heterovalent manganese ions [55]. The magnetization value obtained for $LaMnO_3$ compound can be described in the mentioned model assuming that about 20% of the manganese ions are in 4+ oxidation state, which is in accordance with our previous study [33].

Chemical substitution with alkali elements and chromium ions leads to only slight changes in the structural parameters thus assuming a stabilization of dominant 3+ oxidation state of the chromium ions having ionic radius (0.615Å) similar to that specific for Mn^{3+} ions (0.645Å) [56]. A dominance of chromium ions in 3+ oxidation state should lead to an increase in magnetization of the compounds by positive exchange interaction between Cr^{3+} and Mn^{3+} ions. A formation of positive exchange interactions Cr^{3+}-O-Mn^{3+} is in accordance with the double exchange mechanism used to explain ferromagnetism in compounds having transition metal ions in $3d^3$ and $3d^4$ electron configurations [22,57]. Indeed, the compounds in powder form doped with Na/Cr and K/Cr ions are characterized by the value of in-field magnetization, which is about 40% larger than the magnetization value observed for the initial compound (Figure 6). It should be noted that magnetization data obtained for the compound doped with Li and Cr ions is only slightly changed as compared to the initial compound which is explained by lower chemical homogeneity as compared to other compounds and thus a reduction in positive exchange interactions Cr^{3+}-O-Mn^{3+} and Mn^{3+}-O-Mn^{4+} and stabilization of negative interactions Cr^{3+}-O-Mn^{4+} and Mn^{3+}-O-Mn^{3+}.

Lower value of magnetization obtained for the compounds in ceramic form (Figure 6) can be caused by the smaller size of crystallites leading to a reduction in long-range magnetic order, as well as by a reduced amount of oxygen content formed during high-pressure procedure, which shift the Mn^{3+}/Mn^{4+} ratio out of optimal value. The compounds doped with Na/Cr and K/Cr ions are characterized by the increased value of in-field magnetization as compared to the undoped compound, which is similar to the tendency observed for the powder compounds. The compound doped with Li/Cr ions has lower magnetization among the compounds in both series while a reduction in in-field magnetization is more pronounced in the case of ceramic compounds. The decrease in magnetization observed in Li/Cr doped compound is explained by the Mn^{3+}/Mn^{4+} ratio shifted towards to Mn^{3+} ions as compared to other compounds and a reduced amount of Cr^{3+} ions (Table 3) thus leading to a dominance of negative exchange interactions formed between isovalent manganese ions and Cr^{3+}-O-Mn^{4+}.

There are no publications for the $LaMnO_3$ doped with alkaline elements and chromium together, but articles can be found where at least one similar dopant was used. Firstly, when looking at the case of Ag^+ doping [58], the results presented at 10 K show a similar-shaped peak, however, a slightly larger coercivity as compared to results obtained in our study. The second two most used elements for doping $LaMnO_3$ systems are Sr^{2+} and Ca^{2+} [59]; however, in this case, a slightly higher magnetic field is needed to reach the full saturation. However, it is not too significant as the difference is quite small, most likely due to the similar mechanisms in charge compensation happening in the system

presented in this paper. Lastly, when electroneutrality is maintained during doping in the cases of Ce^{3+} [60] and Cr^{3+} [18] the magnetization results resemble the data presented quite closely, while in other cases, the angle of the magnetization curve, as well as the saturation happening, was slightly different, while, in this case, the magnetic properties are almost identical. Articles on the magnetic particles of $LaMnO_3$ ceramics can also be found. Supelano et al. [61] described the impact of the addition of Mg^{2+} on the magnetic properties of $La_{1-x}Mg_xMnO_3$. They show that the inclusion of Mg in the system induces interactions which arise from the ferromagnetic phase at low temperatures, and it is related to Mn–O–Mn bond angles and Mn–O bond lengths. Similar values of magnetization were observed for ceramics doped with 25% of Mg^{2+}. Zakhvalinskii et al. [62] described the impact of preparation condition of the ceramics on their magnetic properties. They found that $LaMnO_{3+\delta}$ (δ = 0–0.154) ceramic can show different magnetic properties because of the distortion of the cubic perovskite structure induced by time and temperature of annealing.

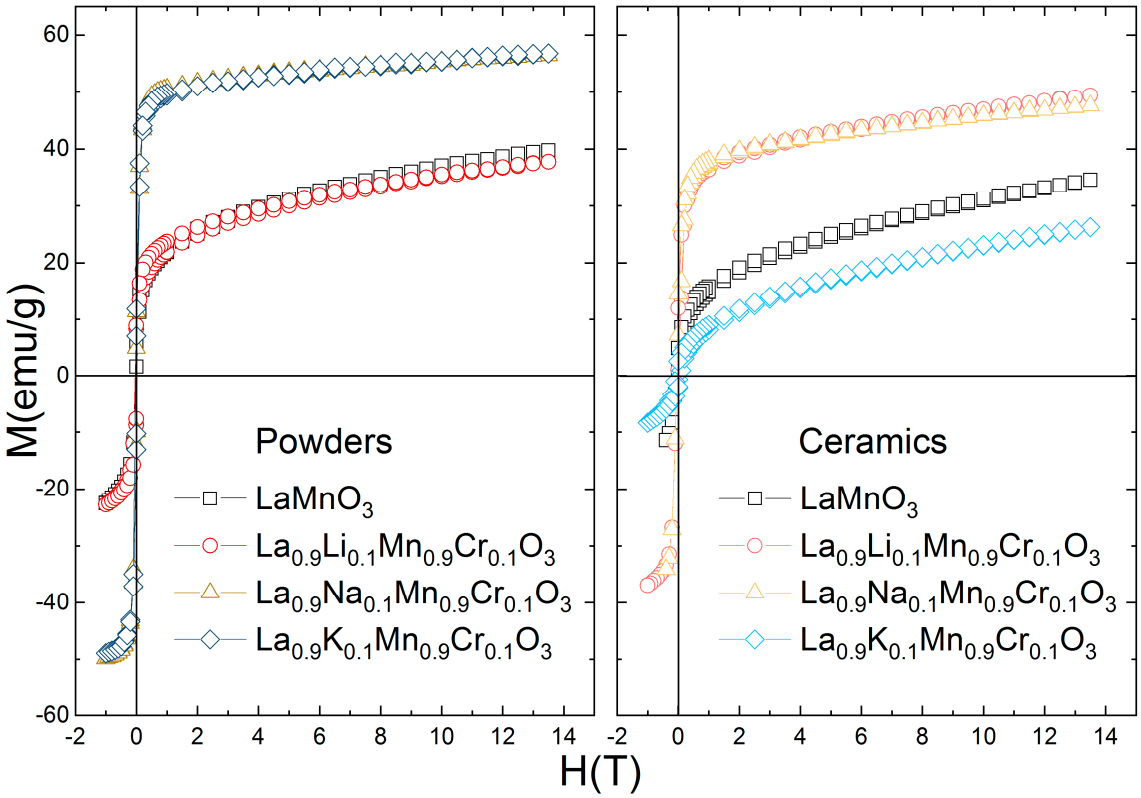

Figure 6. Isothermal magnetization curves of $La_{0.9}A_{0.1}Mn_{0.9}Cr_{0.1}O_3$ (A = Li, Na, K) in powder and ceramic form obtained at T = 5 K.

4. Discussion and Conclusions

Combustion synthesis can be an easy, fast and, above all, scalable method for obtaining multiferroics based on manganese and rare earth ions. Additionally, it has been proven that the structural and magnetic properties can be easily modulated by the addition of various types and amounts of alkali ions, which change the Mn^{3+} to Mn^{4+} ratio. Depending on the dopant used, both the valency of manganese ions (and as shown in this paper also chromium ions) and the distance of these ions from the oxygen ions changes, which has a huge impact on the physical properties of these nanopowders. It has also been shown that under the influence of the high pressure used in the sintering process, the manganite structure, interionic distances, unit cell size and, consequently, also the magnetic properties can be designed. The doping of $LaMnO_3$ with alkali metals and Cr ions allow for the formation of the polar rhombohedral phase, instead of the non-polar orthorhombic one, which is most common in undoped compounds. As such, it would allow for the compound

to potentially be used in multiferroic devices. Furthermore, the distortion in the lattice caused by the aliovalent doping nature, as well as different ionic sizes, could result in higher polarization and magnetization values and, as such, would increase the efficiency of the devices. Furthermore, the differences caused by the alkali element doping on the magnetic structure, as well as on the oxidation state of Cr ions, are noticeable and provide an additional route for material optimization.

Author Contributions: P.G. conceived and planned the experiments and wrote the manuscript with support from other co-authors, R.N. synthesized powders, D.K. (Daniela Kujawa) prepared ceramics, W.S. supervised the project, T.M. performed and analyzed XPS measurements, A.P. performed and analyzed EDS measurements, A.K. supervised the synthesis and analyzed results, A.Y. measured Raman spectra, O.F. analyzed and discussed Raman results, A.Z. measured magnetic properties of powders and ceramics, D.K. (Dmitry Karpinsky) analyzed magnetic properties of powders and ceramics. All authors provided critical feedback and helped shape the research, analysis and manuscript. All authors have read and agreed to the published version of the manuscript.

Funding: This project has received funding from the European Union's Horizon 2020 research and innovation program under the Marie Skłodowska-Curie grant agreement No 778070-TransFerr-H2020-MSCA-RISE-2017.

Institutional Review Board Statement: Not applicable.

Informed Consent Statement: Not applicable.

Data Availability Statement: The data presented in this study are available on request from the corresponding author.

Conflicts of Interest: The authors declare no conflict of interest.

References

1. Schmid, H. Multi-ferroic magnetoelectrics. *Ferroelectrics* **1994**, *162*, 317–338. [CrossRef]
2. Schmid, H. On ferrotoroidics and electrotoroidic, magnetotoroidic and piezotoroidic effects. *Ferroelectrics* **2001**, *252*, 41–50. [CrossRef]
3. Kimura, T. Spiral magnets as magnetoelectrics. *Annu. Rev. Mater. Res.* **2007**, *37*, 387–413. [CrossRef]
4. Tokura, Y.; Seki, S.; Nagaosa, N. Multiferroics of spin origin. *Rep. Prog. Phys.* **2014**, *77*, 076501. [CrossRef] [PubMed]
5. Mostovoy, M. Multiferroics: A whirlwind of opportunities. *Nat. Mater.* **2010**, *9*, 188–190. [CrossRef] [PubMed]
6. Coey, J.M.D.; Viret, M.; Von Molnár, S. Mixed-valence manganites. *Adv. Phys.* **1999**, *48*, 167–293. [CrossRef]
7. Hernández, E.; Sagredo, V.; Delgado, G.E. Synthesis and magnetic characterization of $LaMnO_3$ nanoparticles. *Rev. Mex. Fis.* **2015**, *61*, 166–169.
8. Naish, V.E. Models of Crystal Structures of doped Lanthanum Manganites. *Fiz. Met. Met.* **1998**, *85*, 589–600. [CrossRef]
9. Tokura, Y. Critical features of colossal magnetoresistive manganites. *Rep. Prog. Phys.* **2006**, *69*, 797–851. [CrossRef]
10. Zener, C. Interaction between the d-shells in the transition metals. II. Ferromagnetic compounds of manganese with Perovskite structure. *Phys. Rev.* **1951**, *82*, 403–405. [CrossRef]
11. Phan, M.H.; Yu, S.C. Review of the magnetocaloric effect in manganite materials. *J. Magn. Magn. Mater.* **2007**, *308*, 325–340. [CrossRef]
12. Naik, V.B.; Barik, S.K.; Mahendiran, R.; Raveau, B. Magnetic and calorimetric investigations of inverse magnetocaloric effect in $Pr_{0.46}$ $Sr_{0.54}$ MnO_3. *Appl. Phys. Lett.* **2011**, *98*, 2011–2014. [CrossRef]
13. Bahl, C.R.H.; Velázquez, D.; Nielsen, K.K.; Engelbrecht, K.; Andersen, K.B.; Bulatova, R.; Pryds, N. High performance magnetocaloric perovskites for magnetic refrigeration. *Appl. Phys. Lett.* **2012**, *100*, 121905. [CrossRef]
14. Balli, M.; Jandl, S.; Fournier, P.; Kedous-Lebouc, A. Advanced materials for magnetic cooling: Fundamentals and practical aspects. *Appl. Phys. Rev.* **2017**, *4*, 021305. [CrossRef]
15. Shivakumara, C.; Hegde, M.S.; Srinivasa, T.; Vasanthacharya, N.Y.; Subbanna, G.N.; Lalla, N.P. Synthesis, structure and magnetic properties of Ln1-xAxMnO$_3$ (Ln = Pr, Nd; A = Na, K) from NaCl or KCl flux. *J. Mater. Chem.* **2001**, *11*, 2572–2579. [CrossRef]
16. Sun, Y.; Kamarad, J.; Arnold, Z.; Kou, Z.Q.; Cheng, Z.H. Tuning of magnetocaloric effect in a $La_{0.69}Ca_{0.31}MnO_3$ single crystal by pressure. *Appl. Phys. Lett.* **2006**, *88*, 2004–2007. [CrossRef]
17. Hwang, H.Y.; Palstra, T.T.M.; Cheong, S.W.; Batlogg, B. Pressure effects on the magnetoresistance in doped manganese perovskites. *Phys. Rev. B.* **1995**, *52*, 15046–15049. [CrossRef]
18. Deisenhofer, J.; Paraskevopoulos, M.; Krug von Nidda, H.A.; Loidl, A. Interplay of superexchange and orbital degeneracy in cr-doped (formula presented). *Phys. Rev. B Condens. Matter Mater. Phys.* **2002**, *66*, 054414. [CrossRef]
19. Troyanchuk, I.O.; Bushinsky, M.; Pushkarev, N.; Bespalaya, N.Y. Inhomogeneous magnetic states in the Nd ($Mn_{1-x}Cr_x$) O_3 system. *Phys. Solid State* **2004**, *46*, 1878–1883. [CrossRef]

20. Sun, Y.; Tong, W.; Xu, X.; Zhang, Y. Tuning colossal magnetoresistance response by Cr substitution in $La_{0.67}Sr_{0.33}MnO_3$. *Appl. Phys. Lett.* **2001**, *78*, 643–645. [CrossRef]
21. Raveau, B.; Maignan, A.; Martin, C. Insulator–Metal Transition Induced by Cr and Co Doping in $Pr_{0.5}Ca_{0.5}MnO_3$. *J. Solid State Chem.* **1997**, *130*, 162–166. [CrossRef]
22. Morales, L.; Allub, R.; Alascio, B.; Butera, A.; Caneiro, A. Structural and magnetotransport properties of $LaMn_{1-x}Cr_xO_{3.00}$($0 \leq x \leq 0.15$): Evidence of Mn^{3+}-O-Cr^{3+} double-exchange interaction. *Phys. Rev. B-Condens. Matter Mater. Phys.* **2005**, *72*, 3–6. [CrossRef]
23. Troyanchuk, I.O.; Bushinsky, M.V.; Karpinsky, D.V. Magnetic ordering in manganites substituted by chromium ions. *J. Exp. Theor. Phys.* **2006**, *103*, 580–588. [CrossRef]
24. Troyanchuk, I.O.; Samsonenko, N.V.; Kasper, N.V.; Szymczak, H.; Nabialek, A. Magnetic and Transport Properties of $EuMnO_3$+x Substituted by Ca, Sr and Cr Ions. *Phys. Status Solidi* **1997**, *160*, 195–203. [CrossRef]
25. Gao, T.; Cao, S.; Li, W.; Kang, B.; Yu, L.; Yuan, S.; Zhang, J. Spin glass behavior in the half doped $Pr_{0.5}Ca_{0.5}Mn_{1-x}Cr_xO_3$ system. *Phys. B Condens. Matter* **2009**, *404*, 1283–1286. [CrossRef]
26. Cabeza, O.; Long, M.; Severac, C.; Bari, M.A.; Muirhead, C.M.; Francesconi, M.G.; Greaves, C. Magnetization and resistivity in chromium doped manganites. *J. Phys. Condens. Matter* **1999**, *11*, 2569–2578. [CrossRef]
27. Rivadulla, F.; López-Quintela, M.A.; Hueso, L.E.; Sande, P. Effect of Mn-site doping on the magnetotransport properties of the colossal magnetoresistance compound $La_{2/3}Ca_{1/3}Mn_{1-x}A_xO_3$ (A = Co, Cr; $x \leq 0.1$). *Phys. Rev. B Condens. Matter Mater. Phys.* **2000**, *62*, 5678–5684. [CrossRef]
28. Paul, D.; Anuradha, K.N.; Bhagyashree, K.S.; Bhat, S.V. Electron Magnetic Resonance Studies of Nanosized Nd0.65Ca0.35 $Mn_1-xCrxO_3$ (x = 0, 0.06, 0.1) Manganite. *Appl. Magn. Reson.* **2015**, *46*, 1059–1068. [CrossRef]
29. Kallel, N.; Dhahri, J.; Zemni, S.; Dhahri, E.; Oumezzine, M.; Ghedira, M.; Vincent, H. Effect of Cr doping in $La_{0.7}Sr_{0.3}Mn_{1-x}Cr_xO_3$ with $0 \leq x \leq 0.5$. *Phys. Status Solidi Appl. Res.* **2001**, *184*, 319–325. [CrossRef]
30. Yanchevskii, O.Z.; Belous, A.G.; Tovstolytkin, A.I.; V'yunov, O.I.; Durilin, D.A. Structural, electrical, and magnetic properties of $La_{0.7}Sr_{0.3}Mn_{1-y}Cr_yO_3$. *Inorg. Mater.* **2006**, *42*, 1121–1125. [CrossRef]
31. Xiao, X.; Yuan, S.; Miao, J.; Ren, G.; Yu, G.; Wang, Y.; Yin, S. Tuning colossal magnetoresistance response at roomtemperature by $La_{2/3}$+y$Sr_{1/3}$−y$Mn_{1-y}Cr_yO_3$. *Mater. Lett.* **2007**, *61*, 2315–2318. [CrossRef]
32. Głuchowski, P.; Nikonkov, R.; Tomala, R.; Stręk, W.; Shulha, T.; Serdechnova, M.; Zheludkevich, M.; Pakalaniškis, A.; Skaudžius, R.; Kareiva, A.; et al. Magnetic Properties of $La_{0.9}A_{0.1}MnO_3$ (A: Li, Na, K) Nanopowders and Nanoceramics. *Materials* **2020**, *13*, 1788. [CrossRef]
33. Głuchowski, P.; Nikonkov, R.; Tomala, R.; Stręk, W.; Shulh, T.; Serdechnova, M.; Zarkov, A.; Murauskas, T.; Pakalaniškis, A.; Skaudžius, R.; et al. Impact of Alkali Ions Codoping on Magnetic Properties of $La_{0.9}A_{0.1}Mn_{0.9}Co_{0.1}O_3$ (A: Li, K, Na) Powders and Ceramics. *Appl. Sci.* **2020**, *10*, 8786. [CrossRef]
34. Ekambaram, S.; Patil, K.C.; Maaza, M. Synthesis of lamp phosphors: Facile combustion approach. *J. Alloys Compd.* **2005**, *393*, 81–92. [CrossRef]
35. Fedyk, R.; Hreniak, D.; Łojkowski, W.; Strek, W.; Matysiak, H.; Grzanka, E.; Gierlotka, S.; Mazur, P. Method of preparation and structural properties of transparent YAG nanoceramics. *Opt. Mater.* **2007**, *29*, 1252–1257. [CrossRef]
36. Degen, T.; Sadki, M.; Bron, E.; König, U.; Nénert, G. The high score suite. In *Powder Diffraction*; Cambridge University Press: Cambridge, UK, 2014; Volume 29, pp. S13–S18.
37. Gschneidner, K.A.; Bunzli, J.C.G.; Pecharsky, V.K. *Handbook on the Physics and Chemistry of Rare Earths*; Elsevier: Amsterdam, The Netherlands, 2003.
38. Markovich, V.; Fita, I.; Mogilyansky, D.; Wiśniewski, A.; Puzniak, R.; Titelman, L.; Vradman, L.; Herskowitz, M.; Gorodetsky, G. Effect of particle size on magnetic properties of $LaMnO_{3+\delta}$ nanoparticles. *Superlattices Microstruct.* **2008**, *44*, 476–482. [CrossRef]
39. Suzuki, K.; Koushalya, P.R.; Bhat, S.V. Size Dependent Magnetic Properties of $Nd_{0.7}Ca_{0.3}MnO_3$ Nanomanganite. *IOP Conf. Ser. Mater. Sci. Eng.* **2015**, *73*, 012007.
40. Goveas, L.R.; Bhagyashree, K.S.; Anuradha, K.N.; Bhat, S.V. Size dependence of charge order and magnetism in $Sm_{0.35}Ca_{0.65}MnO_3$. *AIP Adv.* **2021**, *11*, 25313. [CrossRef]
41. Markovich, V.; Fita, I.; Mogilyansky, D.; Wisniewski, A.; Puzniak, P.; Titelman, L.; Vradman, L.; Herskowitz, M.; Gorodetsky, G. Magnetic properties of nanocrystalline $La_{1-x}MnO_{3+\delta}$ manganites: Size effects. *J. Phys. Condens. Matter* **2007**, *19*, 346210. [CrossRef]
42. Głuchowski, P. Pressure -induced changes in the persistent luminescence of $Gd_{2.994}Ce_{0.006}Ga_3Al_2O_{12}$ and $Gd_{2.964}Ce_{0.006}Dy_{0.03}Ga_3Al_2O_{12}$ nanoceramics. *Dalt. Trans.* **2022**, *51*, 5524–5533. [CrossRef]
43. Głuchowski, P.; Tomala, R.; Kowalski, R.; Ignatenko, O.; Witkowski, M.E.; Drozdowski, W.; Stręk, W.; Ryba-Romanowski, W.; Solarz, P. "Frozen" pressure effect in GGAG:Ce^{3+} white light emitting nanoceramics. *Ceram. Int.* **2019**, *45*, 21870–21877. [CrossRef]
44. Iliev, M.; Abrashev, M. Raman spectroscopy of orthorhombic perovskitelike and. *Phys. Rev. B Condens. Matter Mater. Phys.* **1998**, *57*, 2872–2877. [CrossRef]
45. Abrashev, M.V.; Litvinchuk, A.P.; Iliev, M.N.; Meng, R.L.; Popov, V.N.; Ivanov, V.G.; Chakalov, R.A.; Thomsen, C. Comparative study of optical phonons in the rhombohedrally distorted perovskites (formula presented) and (formula presented). *Phys. Rev. B Condens. Matter Mater. Phys.* **1999**, *59*, 4146–4153. [CrossRef]
46. Gupta, K.M.; Gupta, N. Magnetic Materials: Properties and Behaviour. In *Advanced Electrical and Electronics Materials: Processes and Applications*; Scrivener Publishing LLC: Beverly, MA, USA, 2015; pp. 379–421. [CrossRef]

47. Pavlov, V.I.; Bogush, A.K.; Balyko, L.V. Magnetic phase transitions in $LaMnO_{3+\lambda}$. *Cryst. Res. Technol.* **1984**, *19*, 237–245. [CrossRef]
48. Biesinger, M.C.; Payne, B.P.; Grosvenor, A.P.; Lau, L.W.M.; Gerson, A.R.; Smart, R.S.C. Resolving surface chemical states in XPS analysis of first row transition metals, oxides and hydroxides: Cr, Mn, Fe, Co and Ni. *Appl. Surf. Sci.* **2011**, *257*, 2717–2730. [CrossRef]
49. Ilton, E.S.; Post, J.E.; Heaney, P.J.; Ling, F.T.; Kerisit, S.N. XPS determination of Mn oxidation states in Mn (hydr)oxides. *Appl. Surf. Sci.* **2016**, *366*, 475–485. [CrossRef]
50. Amano, M.E.; Betancourt, I.; Arellano-Jimenez, M.J.; Sánchez-Llamazares, J.L.; Sánchez-Valdés, C.F. Magnetocaloric response of submicron (LaAg)MnO_3 manganite obtained by Pechini method. *J. Sol.Gel. Sci. Technol.* **2016**, *78*, 159–165. [CrossRef]
51. Lv, Y.; Li, Z.; Yu, Y.; Yin, J.; Song, K.; Yang, B.; Yuan, L.; Hu, X. Copper/cobalt-doped $LaMnO_3$ perovskite oxide as a bifunctional catalyst for rechargeable Li-O_2 batteries. *J. Alloys Compd.* **2019**, *801*, 19–26. [CrossRef]
52. Lee, Y.N.; Lago, R.M.; Fierro, J.L.G.; Cortés, V.; Sapiña, F.; Martínez, E. Surface properties and catalytic performance for ethane combustion of $La_{1-x}K_xMnO_{3+\delta}$ perovskites. *Appl. Catal. A Gen.* **2001**, *207*, 17–24. [CrossRef]
53. Wei, Z.-X.; Wei, L.; Gong, L.; Wang, Y.; Hu, C.-W. Combustion synthesis and effect of $LaMnO_3$ and La0.8Sr0.2MnO_3 on RDX thermal decomposition. *J. Hazard. Mater.* **2010**, *177*, 554–559. [CrossRef] [PubMed]
54. Yang, L.; Hu, J.; Tian, G.; Zhu, J.; Song, Q.; Wang, H.; Zhang, C. Efficient Catalysts of K and Ce Co-Doped LaMnO3for NOx-Soot Simultaneous Removal and Reaction Kinetics. *ACS Omega* **2021**, *6*, 19836–19845. [CrossRef]
55. García-Muñoz, J.; Fontcuberta, J.; Martinez, B.; Seffar, A.; Pinol, S.; Obradors, X. Magnetic frustration in mixed valence manganites. *Phys. Rev. B-Condens. Matter Mater. Phys* **1997**, *55*, R668–R671. [CrossRef]
56. Shannon, R.D. Revised effective ionic radii and systematic studies of interatomic distances in halides and chalcogenides. *Acta Cryst.* **1976**, *A32*, 751–766. [CrossRef]
57. Georgalas, C.; Samartzis, A.; Biniskos, N.; Syskakis, E. Effects of Cr-doping on the Jahn-Teller, the orthorhombic to rhombohedral, and the magnetic transitions in $LaMn_{1-x}Cr_xO_3$ compounds. *Phys. B Condens. Matter* **2020**, *586*, 412101. [CrossRef]
58. Afify, M.S.; El Faham, M.M.; Eldemerdash, U.; El Rouby, W.M.; El-Dek, S. Room temperature ferromagnetism in Ag doped $LaMnO_3$ nanoparticles. *J. Alloys Compd.* **2020**, *861*, 158570. [CrossRef]
59. Branković, Z.; Đuris, K.; Radojković, A.; Bernik, S.; Jagličić, Z.; Jagodic, M.; Vojisavljević, K.; Branković, G. Magnetic properties of doped $LaMnO_3$ ceramics obtained by a polymerizable complex method. *J. Sol-Gel Sci. Technol.* **2010**, *55*, 311–316. [CrossRef]
60. Das, S.; Poddar, A.; Roy, B.; Giri, S. Studies of transport and magnetic properties of Ce-doped $LaMnO_3$. *J. Alloys Compd.* **2004**, *365*, 94–101. [CrossRef]
61. Supelano, G.I.; Barón-González, A.J.; Santos, A.S.; Ortíz, C.; Gómez, J.A.M.; Vargas, C.A.P. Effect of Mg addition on $LaMnO_3$ ceramic system. *J. Mater. Res. Technol.* **2018**, *7*, 77–81. [CrossRef]
62. Zakhvalinskiĭ, V.S.; Laiho, R.; Lisunov, K.G.; Lähderanta, E.; Petrenko, P.A.; Stepanov, Y.P.; Salminen, J.; Stamov, V.N. Preparation and magnetic properties of $LaMnO_{3+\delta}$ ($0 \leq \delta \leq 0.154$). *Phys. Solid State* **2006**, *48*, 2300–2309. [CrossRef]